Euler Solutions for Airfoil/Jet/Ground-Interaction Flowfields

Ramesh K. Agarwal* and Jerry E. Deese†
McDonnell Douglas Research Laboratories, St. Louis, Missouri

Airfoil/jet/ground-interaction flowfields are calculated by solving Euler equations on body-conforming curvilinear grids. For these computations, Jameson's Euler code (FLO-53) based on an explicit Runge-Kutta time-marching finite-volume procedure is modified. Euler equations are preconditioned for computing almost incompressible flows. Euler equations capture the vortex formation behind the jet and most of the airfoil/jet/ground-plane interaction, except the effect of entrainment. Reasonable agreement is obtained between the calculated and experimental values of the lift on the airfoil for moderate values of jet-velocity to freestream-velocity ratio.

Nomenclature

A,B	= Jacobian matrices defined in Eq. (2)
c	= chord length of the airfoil
c_μ	= momentum coefficient
C_L, C_p	= lift and pressure coefficients, respectively
d_j	= jet width
E	= total energy
F,G	= flux vectors defined by Eq.(1)
h	= jet height above the ground plane
H	= total enthalpy
J	= Jacobian of transformation between Cartesian coordinate system (x,y) and curvilinear coordinate system (ξ,η)
M	= Mach number
p	= pressure
q	= conservative flow variable defined by Eq. (1)
R	= nonsingular positive definite matrix defined by Eq. (12)
Re_c	= Reynolds number based on airfoil chord
t	= time
u,v	= velocity components
V	= absolute velocity
V_R	= velocity ratio (V_j/V_∞)
(x,y)	= Cartesian coordinates
x_j	= location of jet centerline from leading edge of the airfoil
α	= angle of attack
ρ	= density
$\lambda_1,\lambda_2,\lambda_3$	= eigenvalues defined by Eq. (7)
(ξ,η)	= curvilinear coordinates
τ	= thickness of the airfoil

Superscript

$(\bar{\ })$	= nondimensional value

Subscripts

∞	= value in the freestream
j	= value in the jet

Introduction

SUCCESSFUL design and development of V/STOL aircraft require accurate prediction of forces and moments caused by jet-induced effects during takeoff. During hover and transition to and from conventional forward flight, extensive aerodynamic interactions occur between the lifting jets and the flow around the aircraft. In this paper we study the aerodynamics of a model high-lift system that consists of an airfoil in ground effect with a jet issuing from its undersurface, using the Euler equations to describe the flowfields. Previous theoretical study on this problem (in the absence of ground plane) has been conducted by Tavella and Karamcheti,[1] who formulated a potential flow model similar to that used in jet-flap theory; experiments have been performed recently by Krothapalli et al.[2]

As shown in Fig. 1 (Case I), in forward flight a large recirculating flow region exists behind the jet, resulting in low pressures on the lower surface of the airfoil. As the jet-velocity to freestream-velocity ratio V_R increases, this separated flow region appears even farther upstream of the jet [Fig. 1 (Case II)], resulting in a greater suckdown force.

Figure 2 shows the flow structure (Type I or II in Fig. 1) as a function of the velocity ratio and the height above the ground plane, based on the experimental observations of Krothapalli et al.[2] It should be noted that in Fig. 2, the momentum coefficient $c_\mu = (\rho_j V_j^2 d_j/\rho_\infty V_\infty^2 c)$ should ordinarily be employed as a nondimensional parameter instead of V_j/V_∞. In the experiments of Krothapalli et al., $V_j/V_\infty = 1$, $d_j/c = 2.02$, and $x_j = 0.5$; thus Fig. 2 truly holds for these values of jet density, jet width, and jet location on the airfoil surface.

In a potential flow model (in the absence of ground plane), as shown in Fig. 3, the jet is idealized as an infinitely thin sheet, and the separated flow behind it is simulated with a dead air region of constant pressure (equal to the freestream pressure) bounded by a free streamline that is part of the airfoil surface and the jet. The potential flow model is inadequate in many respects: 1) the pressure in the wake is assumed equal to the pressure of the freestream, causing the wake to be open and infinite as shown in Fig. 3; 2) it cannot include the effects of the vortex formation behind the jet that is responsible for low pressures on the undersurface of the airfoil; 3) in the presence of a ground plane, there is no simple way to incorporate the jet/ground interaction effects on the flowfield around the airfoil.

A better physical model of the airfoil/jet/ground-interaction flowfield is provided by the Euler equations, which can describe the vortex formation behind the jet and include the effect of jet/ground-plane interaction on the flowfield around the airfoil. However, the effects of entrainment are ignored in the Euler formulation. The airfoil/jet/ground-interaction flowfield is calculated by solving Euler equations on body-conforming curvilinear grids.

Numerical Solution Algorithm

A modular solution approach is adopted in which an independently generated grid is coupled with the flow solver.

Received April 3, 1985; revision received Feb. 5, 1986.

*Senior Scientist. Associate Fellow AIAA.
†Scientist. Member AIAA.

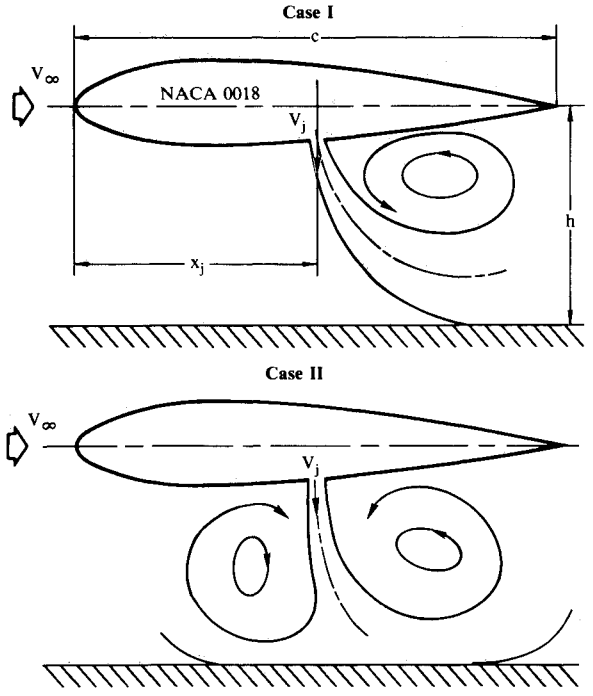

Fig. 1 Schematic of flow around an airfoil in ground effect with a jet issuing from its undersurface.

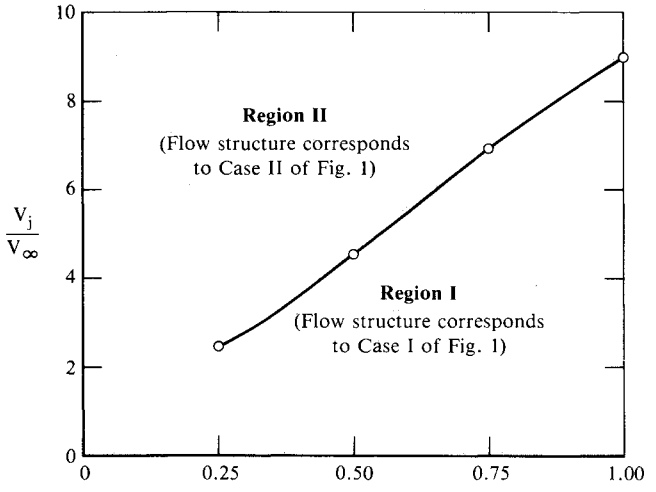

Fig. 2 Experimentally observed regions (corresponding to the flow structures in Fig. 1) as a function of velocity ratio (V_j/V_∞) and the height above the ground plane (h/c).

An algebraic grid-generation code, conceptually based on the multisurface method, is employed for coordinate generation.[3] To solve the Euler equations, the two-dimensional Euler code (FLO-53) developed by Jameson et al.[4] is used. The considerable control provided by the algebraic grid-generation method is effectively utilized in achieving an efficient distribution of grid points in the flow domain. Modifications to the code are made for treating far-field, airfoil, ground-plane, and jet-region boundary conditions. For calculating low subsonic flows, the numerical scheme is modified as suggested by Turkel,[5] so that singular behavior is not encountered as the freestream Mach number M_∞ approaches zero.

The following review outlines the characteristics of the code that pertain to the results described in this paper.

Let p, ρ, (u,v), E, and H denote pressure, density, the Cartesian velocity components, total energy, and total enthalpy, respectively. Let p_∞, ρ_∞, V_∞, and H_∞ denote the pressure, density, velocity, and total enthalpy, respectively, in the freestream. In FLO-53, p_∞, ρ_∞, $\sqrt{p_\infty/\rho_\infty}$, and (p_∞/ρ_∞) are used to nondimensionalize p, ρ, (u,v), and (E,H), respectively, in contrast to the standard formulations in which p, ρ, (u,v), and (E,H) are nondimensionalized by $\frac{1}{2}\rho_\infty V_\infty^2$, ρ_∞, V_∞, and V_∞^2, respectively. As indicated by Briley et al,[6] the standard nondimensionalization of the compressible Euler equations encounters singular behavior as the Mach number approaches zero. However, with the nondimensionalization employed in FLO-53, the compressible Euler equations reduce to incompressible form as $M_\infty \to 0$. In FLO-53, the nondimensional variables are defined as follows:

$$\bar{\rho}=\rho/\rho_\infty,\ \bar{p}=p/p_\infty,\ (\bar{u},\bar{v})=(u,v)/\sqrt{p_\infty/\rho_\infty}$$

$$\bar{E}=\rho_\infty(E-H_\infty)/p_\infty,\ \bar{H}=\rho_\infty(H-H_\infty)/p_\infty$$

$$(\bar{x},\bar{y})=(x,y)/L,\ \bar{t}=t/(L\sqrt{\rho_\infty/p_\infty})$$

Let $\xi=\xi(\bar{x},\bar{y})$ and $\eta=\eta(\bar{x},\bar{y})$ describe the coordinate transformation between the Cartesian system $(\bar{x},\bar{y})$ and the body-oriented curvilinear system (ξ,η). In the (ξ,η) coordinate system, the Euler equations can be written

$$\frac{\partial\bar{q}}{\partial\bar{t}}+\frac{\partial\bar{F}}{\partial\xi}+\frac{\partial G}{\partial\eta}=0 \tag{1}$$

where

$$\bar{q}=qJ,\ J=\bar{x}_\xi\bar{y}_\eta-\bar{x}_\eta\bar{y}_\xi,\ \bar{F}=\bar{y}_\eta F-\bar{x}_\eta G,\ \bar{G}=-\bar{y}_\xi F+\bar{x}_\xi G$$

Also

$$q=\begin{bmatrix}\bar{\rho}\\ \bar{\rho}\bar{u}\\ \bar{\rho}\bar{v}\\ \bar{\rho}\bar{E}\end{bmatrix},\quad F=\begin{bmatrix}\bar{\rho}\bar{u}\\ \bar{\rho}\bar{u}^2+\bar{p}\\ \bar{\rho}\bar{u}\bar{v}\\ \bar{\rho}\bar{u}\bar{H}\end{bmatrix},\quad G=\begin{bmatrix}\bar{\rho}\bar{v}\\ \bar{\rho}\bar{v}\bar{u}\\ \bar{\rho}\bar{v}^2+\bar{p}\\ \bar{\rho}\bar{v}\bar{H}\end{bmatrix}$$

In FLO-53, Eq. (1) is solved by a finite-volume, explicit, four-step, Runge-Kutta time-stepping scheme. The use of an explicit scheme places a restriction on the time step, as seen by the following analysis.

Equation (1) can be written in quasilinear form as

$$\frac{\partial\bar{q}}{\partial\bar{t}}+A\frac{\partial\bar{q}}{\partial\xi}+B\frac{\partial\bar{q}}{\partial\eta}=0 \tag{2}$$

where $A=\partial\bar{F}/\partial\bar{q}$ and $B=\partial\bar{G}/\partial\bar{q}$ are the Jacobian matrices. Since $\bar{F}$ and $\bar{G}$ are homogenous functions of degree one in $\bar{q}$, one can write

$$\bar{F}=A\bar{q},\qquad \bar{G}=B\bar{q} \tag{3}$$

In the finite-volume scheme, Eq. (1) is integrated over a cell of area Ω and boundary $\partial\Omega$ to obtain

$$\int_\Omega\int\frac{\partial\bar{q}}{\partial\bar{t}}d\Omega+\int_\Omega\int\left(\frac{\partial\bar{F}}{\partial\xi}+\frac{\partial\bar{G}}{\partial\eta}\right)d\Omega=0 \tag{4}$$

Using Green's theorem to transform the second area integral to a line integral, and noting that $\bar{q}$ is, in effect, the average value for the cell, Eq. (4) can be written

$$\frac{d\bar{q}_{ij}}{d\bar{t}}+\oint_{\partial\Omega}(\bar{F}d\eta-\bar{G}d\xi)=0 \tag{5}$$

or

$$\frac{d\bar{q}_{ij}}{d\bar{t}}+\oint_{\partial\Omega}(Ad\eta-Bd\xi)\bar{q}=0 \tag{6}$$

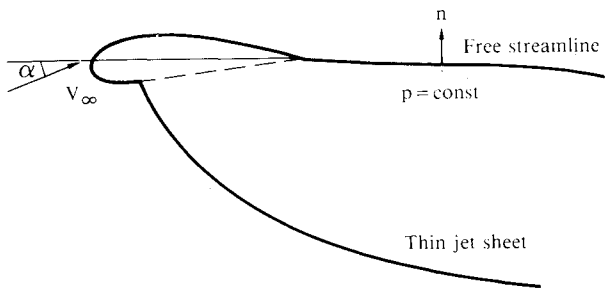

Fig. 3 Potential flow model based on jet-flap theory.

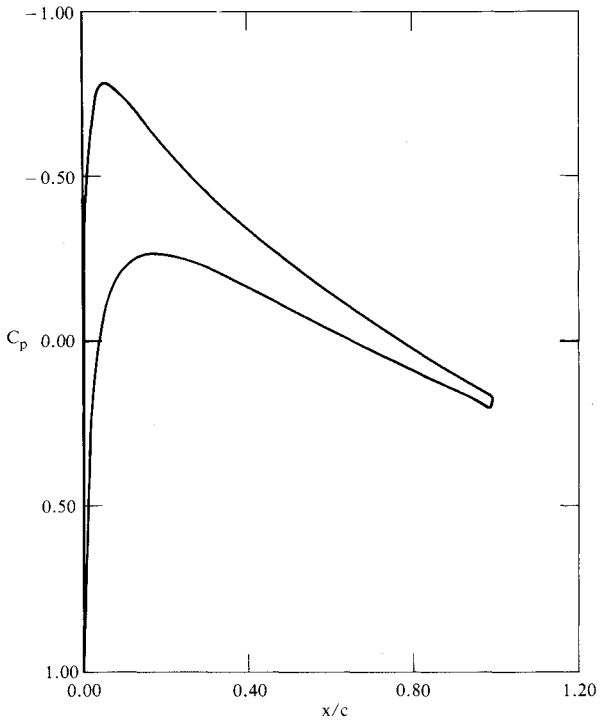

Fig. 4 Computed pressure distribution on a 12%-thick Joukowski airfoil; $M_\infty = 0.01$, $\alpha = 2$ deg.

In Eq. (6), $(A\Delta\eta - B\Delta\xi)$ represents the Jacobian matrix for fluxes across the faces of a rectangular cell of sides $\Delta\xi$ and $\Delta\eta$. Since Eq. (2) is a hyperbolic system, $(A\Delta\eta - B\Delta\xi)$ can be diagonalized by a similarity transformation

$$Q^{-1}(A\Delta\eta - B\Delta\xi)Q = \Lambda = \begin{bmatrix} \lambda_1 & 0 & 0 & 0 \\ 0 & \lambda_1 & 0 & 0 \\ 0 & 0 & \lambda_2 & 0 \\ 0 & 0 & 0 & \lambda_3 \end{bmatrix} \tag{7}$$

where

$$\lambda_1 = au - bv$$

$$\lambda_2 = au - bv + c\sqrt{a^2 + b^2}$$

$$\lambda_3 = au - bv - c\sqrt{a^2 + b^2} \tag{8}$$

$a = (y_\eta \Delta\eta + y_\xi \Delta\xi)$, $b = (x_\xi \Delta\xi + x_\eta \Delta\eta)$, and c is the speed of sound. The spectral radius of $(A\Delta\eta - B\Delta\xi)$ is the largest eigenvalue, that is λ_2. Now, for an explicit multistep Runge-Kutta method used in integrating Eq. (6), we can write the stability criteria as

$$\Delta\bar{t} \cdot \lambda_2 \leq K \cdot J \tag{9}$$

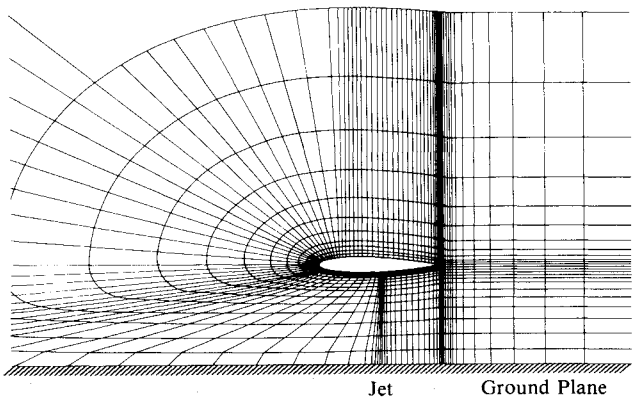

Fig. 5 Algebraically generated grid around a NACA 0018 airfoil in ground effect with a jet issuing from its undersurface.

where K depends on the parameters of the Runge-Kutta scheme.

For a square cell $\Delta\xi = \Delta\eta = 1$, then the restriction on the time step can be written

$$\Delta\bar{t} \leq \frac{K \cdot J}{|au - bv| + c\sqrt{a^2 + b^2}} \leq \frac{K \cdot J}{|au| + |bv| + c\sqrt{a^2 + b^2}} \tag{10}$$

From Eq. (10), it is clear that the time step is bounded by $1/c$. However, the physical properties change over time scales of order $1/u$, which is much larger than $1/c$ for low subsonic flows. As a result, a very large number of time steps are required to make a significant change in the evolution of the solution to steady state. Turkel[5] has suggested a modification to the Runge-Kutta scheme that makes the time step $\Delta\bar{t}$ independent of c at low Mach numbers. The modification is applicable only for computing the steady-state solution. Turkel[5] replaces Eq. (1) by

$$R^{-1}\frac{\partial \bar{q}}{\partial \bar{t}} + \frac{\partial \bar{F}}{\partial \xi} + \frac{\partial \bar{G}}{\partial \eta} = 0 \tag{11}$$

where R is a nonsingular positive definite matrix chosen such that the eigenvalues of RA and RB are independent of c. There are many possible choices for R; Turkel[5] suggests the following form for R:

$$R = I + eQ \tag{12}$$

where I is a 4×4 unit diagonal matrix and

$$Q = \begin{bmatrix} S^2 & -u & -v & 1 \\ uS^2 & -u^2 & -uv & u \\ vS^2 & -uv & -v^2 & v \\ hS^2 & -uh & -vh & h \end{bmatrix} \tag{13}$$

$$e = \frac{\gamma - 1}{c^2}(\theta^2 - 1), \quad \theta = \frac{z^2}{c^2}, \quad S^2 = (u^2 + v^2),$$

$$h = S^2 + \frac{c^2}{\gamma - 1}, \quad z^2 = \max(\epsilon, u^2 + v^2)$$

Here ϵ is introduced so that R^{-1} is not singular at stagnation points. Turkel[5] recommends $\epsilon = 0.01c$ to obtain reasonable rates of convergence. With the choice of R given by Eq. (12), the spectral radius of the Jacobian matrix $(RA\Delta\eta - RB\Delta\xi)$ can now be determined by following the analysis outlined

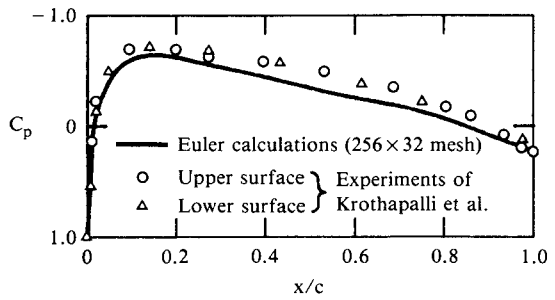

Fig. 6 Pressure distribution on a NACA 0018 airfoil; $M_\infty = 0.0588$, $\alpha = 0$ deg.

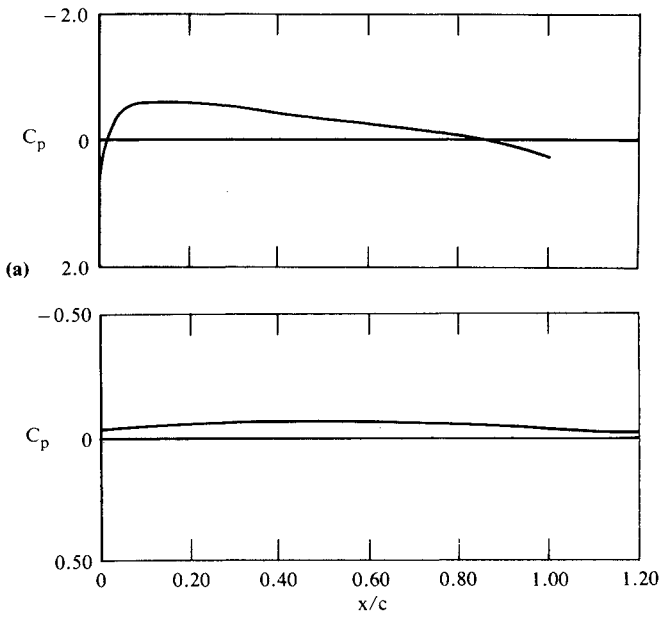

Fig. 7 Computed pressure distribution on a) NACA 0018 airfoil and b) the ground plane, $M_\infty = 0.0588$, $V_R = 0$, $\alpha = 0$ deg, $h/c = 1.0$.

before. The largest eigenvalue of $(RA - RB)$ is given by

$$\lambda = \left\{ |au - bv|(1+\theta^2) + \sqrt{(1-\theta^2)(au-bv)^2 + 4(a^2+b^2)z^2} \right\} \Big/ 2 \tag{14}$$

For $\theta = 1$, we obtain $\lambda = |au - bv| + c\sqrt{a^2+b^2} = \lambda_2$ of Eq. (8). But for $\theta = 0(\epsilon)$, which is the case at low Mach numbers, Eq. (14) gives $\lambda = 0(\epsilon)$. Hence, at very low Mach numbers the largest eigenvalue [and therefore, from Eq. (9), the time step] are independent of the speed of sound. For calculating low subsonic flows, the preconditioned form of the Euler equations, Eq. (11), allows use of a much larger time step and enhances the convergence to steady state.

For cell (i,j) with $\Delta\xi = \Delta\eta = 1$, the finite-volume discretization of Eq. (11) takes the form

$$R_{ij}^{-1}\frac{d\bar{q}_{ij}}{dt} + \bar{F}_{i+1/2,j} - \bar{F}_{i-1/2,j} + \bar{G}_{i,j+1/2} - \bar{G}_{i,j-1/2} = 0 \tag{15}$$

Suppressing the subscript (i,j) and noting $\bar{q} = qJ$, Eq. (15) is written

$$R^{-1}\frac{d(Jq)}{dt} + \mathfrak{F}q = 0 \tag{16}$$

Second- and fourth-order artificial viscosity terms $\mathfrak{D}\bar{q}$, as proposed by Jameson et al.,[4] are added to Eq. (16) to suppress the tendency for odd- and even-point decoupling and to prevent oscillations in regions of high pressure gradient. Equation (16) then becomes

$$R^{-1}\frac{dq}{dt} + Pq = 0 \tag{17}$$

where

$$Pq = \mathfrak{F}q + \mathfrak{D}q$$

For integrating Eq. (17), the classical fourth-order Runge-Kutta scheme is used in the following manner.

At time level n, set $q^{(0)} = q^n$ and calculate $R^{(0)} = R(q^{(0)})$

$$q^{(1)} = q^{(0)} - \frac{\Delta t}{2}R^{(0)}Pq^{(0)}$$

$$R^{(1)} = R(q^{(1)})$$

$$q^{(2)} = q^{(0)} - \frac{\Delta t}{2}R^{(1)}Pq^{(1)}$$

$$R^{(2)} = R(q^{(2)})$$

$$q^{(3)} = q^{(0)} - \Delta t R^{(2)}Pq^{(2)}$$

$$R^{(3)} = R(q^{(3)})$$

$$q^{(4)} = q^{(0)} - \frac{\Delta t}{6}\left\{R^{(0)}Pq^{(0)} + 2R^{(1)}Pq^{(1)} + 2R^{(2)}Pq^{(2)} + R^{(3)}Pq^{(3)}\right\}$$

$$q^{n+1} = q^{(4)} \tag{18}$$

For calculating low subsonic flows, the FLO-53 modification essentially involves the changes in Runge-Kutta scheme given in Eq. (18), with matrix R defined by Eq. (12).

All other features of the code remain the same as described in Refs. 3 and 4.

Numerical Results

Low subsonic flow past a Joukowski airfoil: $M_\infty = 0.01$ and 0.2, and $\alpha = 2$ deg.

Calculations were performed to evaluate the accuracy and convergence characteristics of the modified FLO-53 code for computing almost incompressible flow. Two main differences were observed in the performance of the code at $M_\infty = 0.01$ and 0.2: 1) to obtain the correct value of lift, a reduction in the average residual of approximately seven orders of magnitude was required at $M_\infty = 0.01$ compared to a comparable reduction of four orders of magnitude required at $M_\infty = 0.2$; 2) to obtain the converged solution at $M_\infty = 0.01$, 12,700 iterations were needed, compared to 700 iterations at $M_\infty = 0.2$. CPU time is 1.6 s/iteration on a 257×33 mesh.

The lift coefficient for a symmetric Joukowski airfoil at angle of attack in subsonic flow is given by[7]

$$C_L = \frac{2\pi(1 + 0.77\tau)\sin\alpha}{\sqrt{1 - M_\infty^2}} \tag{19}$$

where τ is the airfoil thickness. At $M_\infty = 0.2$ and $\alpha = 2$ deg, Eq. (19) gives a lift coefficient of 0.2444 for an airfoil with a 12%-thickness ratio. The present Euler calculation predicts a lift coefficient of 0.2395 under these conditions, within 3% of theoretical value.

At $M_\infty = 0.01$ and $\alpha = 2$ deg, Eq. (19) gives a lift coefficient of 0.2395 while the numerical value is 0.2182, within 8.9% of the theoretical result. Figure 4 shows the pressure

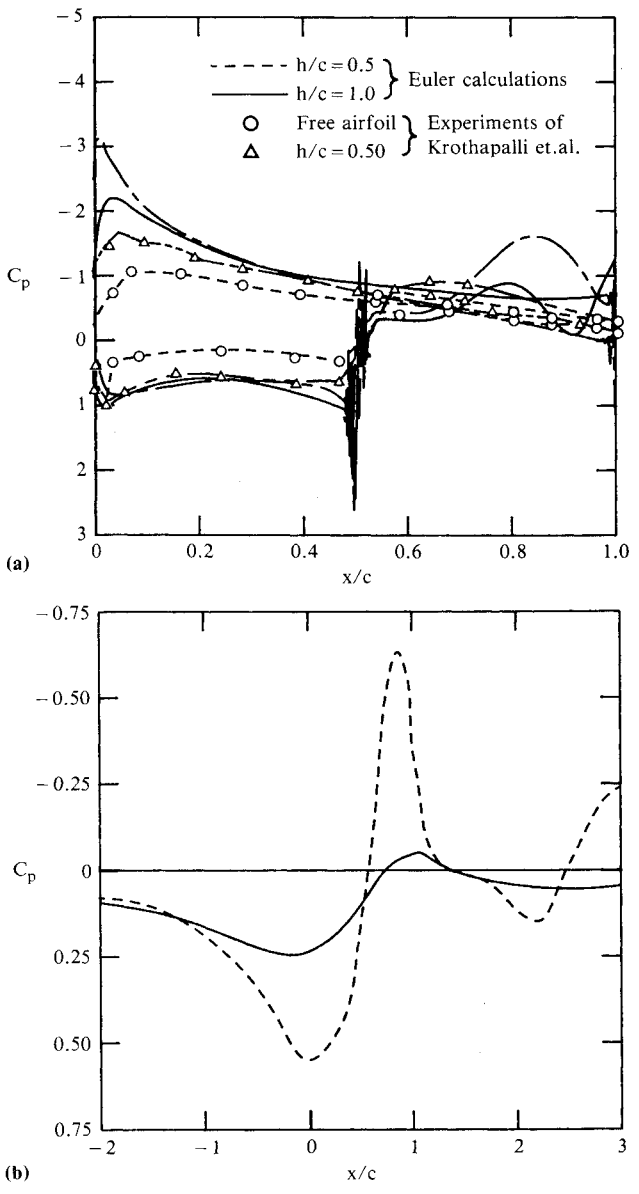

Fig. 8 Pressure distribution on a) NACA 0018 airfoil and b) the ground plane; $M_\infty = 0.0588$, $V_R = 2.0$, $\alpha = 0$ deg.

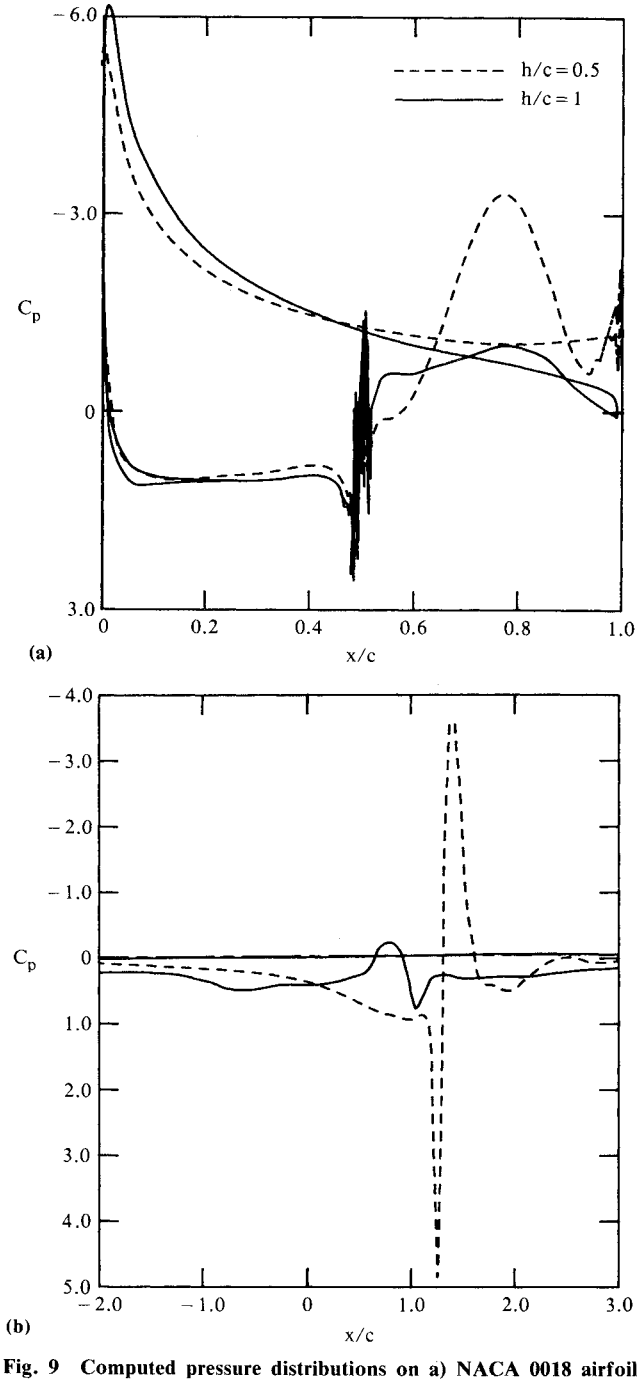

Fig. 9 Computed pressure distributions on a) NACA 0018 airfoil and b) the ground plane; $M_\infty = 0.0588$, $\alpha = 0$ deg, $V_R = 4.0$.

distribution on the airfoil at $M_\infty = 0.01$. For this calculation, pressure differences as small as 10^{-7} are significant and affect the value of the lift coefficient because of the very small value (7×10^{-5}) of the normalized freestream dynamic pressure.

These calculations show that although FLO-53 can be used for almost incompressible flows, a significant penalty is paid in the excessively large number of iterations required to obtain an accurate solution. Even the use of multigrid strategy may not reduce the computational time to a reasonable level. Alternative procedures should be employed for calculating incompressible flows.

Low subsonic flow past a NACA 0018 airfoil in ground effect with a jet issuing from its undersurface: $M_\infty = 0.0588$, $h/c = 0.5$ and 1, $0 \le V_R \le 4$.

Figure 5 shows the near-field view of a typical grid around a NACA 0018 airfoil in the presence of the ground plane and the jet. Grid points are clustered near the leading and trailing edges and in the jet region. Although the computational region between the airfoil and the ground plane is confined to one chord length, the grid is stretched over 12 chords from the airfoil surface to the upper far-field boundary.

Figure 6 shows the pressure distribution on a free airfoil (in the absence of the jet and the ground plane). Agreement between the Euler calculations and the experimental data is fairly good considering that the NACA 0018 is a thick airfoil; at Reynolds number $Re_c = 2 \times 10^5$ (experimental value), the viscous effects become quite important.

Figure 7a shows the computed pressure distribution on the airfoil in ground effect in the absence of the jet. Since the angle of attack $\alpha = 0$ deg, the influence of the ground plane tends to generate a small positive lift on the airfoil ($C_L = 0.02$). Figure 7b shows the distribution of the ground plane pressure, which is greater than the freestream pressure. As the flow approaches the airfoil along the ground plane, there is a slight deceleration and pressure rise. Along the ground plane just beneath the airfoil, the flow accelerates because of area constriction, as in a converging nozzle. Downstream of the trailing edge, the flow decelerates as a

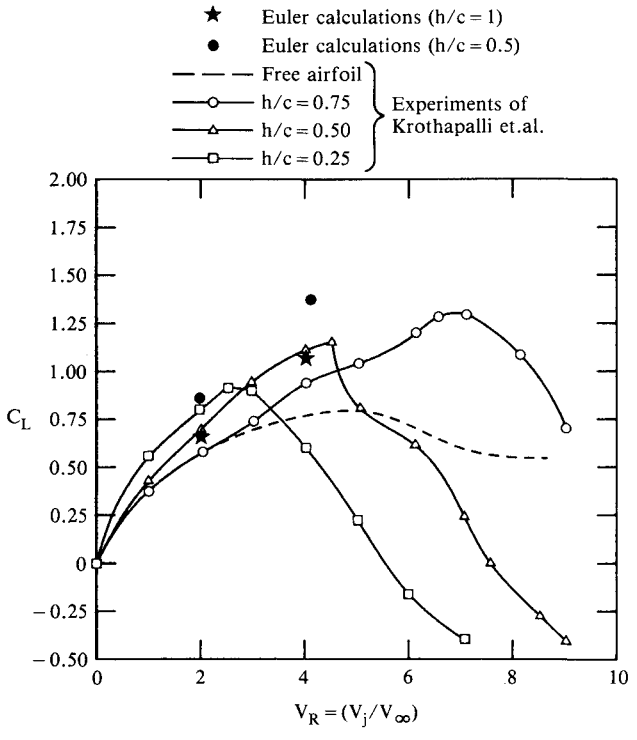

Fig. 10 Variation of lift coefficient (C_L) with velocity ratio (V_R) for a NACA 0018 airfoil in ground effect; $M_\infty = 0.0588$, $\alpha = 0$ deg.

result of the airfoil downwash before returning to the freestream condition.

Figure 8a shows the pressure distribution on the upper and lower surface of the airfoil in the presence of a jet with $V_R = 2$ for varying heights above the ground plane. According to the experiments of Krothapalli et al.,[2] for $h/c \geq 0.5$ and $V_R = 2$, the flow structure corresponds to Case I of Fig. 1. Euler calculations also predict a vortexlike structure behind the jet. As shown in Fig. 8a, the computed inviscid pressure distribution is in qualitative agreement with the experimental data on both the upper and lower surfaces of the airfoil. Inviscid calculations do not include the effect of entrainment, which appears to be significant in these flows, and hence the discrepancy between the inviscid calculations and the experimental data. Figure 8b shows the computed pressure distribution on the ground plane for this case.

Figure 9a shows the computed pressure distribution on the upper and lower surface of the airfoil with $V_R = 4$. As the jet velocity increases, the extent of the separated flow region behind the jet increases, resulting in a large suckdown force. Furthermore, the impact of a high-velocity jet on the ground gives rise to large ground-plane pressure as shown in Fig. 9b. These calculations could not be compared with the experiments because of lack of pressure data on the airfoil surface for this case. Comparing Figs. 8a and 9a, we note that the pressure distributions on the airfoil surface are qualitatively similar at $V_R = 2$ and $V_R = 4$.

Figure 10 shows the variation of lift-coefficient C_L with V_R. The computed value of C_L is in reasonable agreement with the measured value. As expected, the computed value of lift is higher at $h/c = 0.5$ compared to that at $h/c = 1.0$.

Conclusions

Based on this study, the following conclusions can be drawn:

1) Euler equations capture most of the physics of airfoil/jet/ground-interaction problem except the effect of entrainment.

2) Euler equations can be used to capture vortex formation in separated flows.

3) For moderate values of V_R (=jet-velocity to freestream-velocity), Euler equations can give a reasonable estimate of the lift on the airfoil in ground effect. Calculations and the experiments both show that the lift force increases almost linearly with V_R for $0 \leq V_R \leq 4$ and the ground-plane pressure remains positive. For $V_R \geq 4$, the Euler equations are not appropriate for calculating the forces on the airfoil. Viscous effects predominate—Reynolds-averaged Navier-Stokes equations with an appropriate turbulence closure should be employed as a physical model for $V_R > 4$. According to the experiments of Krothapalli et al.,[2] C_L starts decreasing for $4 < V_R < 7$ and then becomes nearly constant for $V_R > 7$.

4) Compressible Euler equations can be used to calculate almost incompressible flow ($M_\infty = 0.01$) without encountering singular behavior by employing a nonstandard nondimensionalization for the velocity and pressure variables. Convergent steady-state solutions for almost incompressible flow can be obtained by employing the preconditioning suggested by Turkel.[5]

Acknowledgments

This work was conducted under the McDonnell Douglas Independent Research and Development Program. The authors are grateful to Prof. A. Krothapalli of Florida State University for providing the experimental information used in this paper.

References

[1]Tavella, D.A. and Karamcheti, K., "Aerodynamics of an Airfoil with a Jet Issuing from Its Surface," AIAA Paper 82-0220, 1982.

[2]Krothapalli, A., Leopold, D., and Koenig, D., "An Experimental Investigation of Flow Surrounding an Airfoil with a Jet Exhausting from Lower Surface," NASA CR-166131, 1981.

[3]Agarwal, R.K. and Deese, J.E., "Numerical Solution of the Euler Equations for Flow Past an Airfoil in Ground Effect," AIAA Paper 84-0051, 1984.

[4]Jameson, A., Schmidt, W., and Turkel, E., "Numerical Solutions of the Euler Equations by Finite Volume Methods Using Runge-Kutta Time-Stepping Schemes," AIAA Paper 81-1259, 1981.

[5]Turkel, E., "Fast Solutions to the Steady State Compressible and Incompressible Fluid Dynamic Equations," ICASE Rept. 84-28, NASA CR-172416, 1984.

[6]Briley, W.R., McDonald, H., and Shamroth, S.J., "A Low Mach Number Euler Formulation and Application to Time-Iterative LBI Schemes," *AIAA Journal*, Vol. 21, Oct. 1983, pp. 1467-1468.

[7]Karamcheti, K., *Principles of Ideal-Fluid Aerodynamics*, John Wiley & Sons, New York, 1966, p. 485.